

Numerical study of a turbulent hydrogen flame in oxy-combustion regimes

A. WAWRZAK*, A. TYLISZCZAK

Częstochowa University of Technology
Al. Armii Krajowej 21
42-201 Częstochowa, Poland
e-mails: awawrzak@imc.pcz.pl, atyl@imc.pcz.pl

THIS PAPER PRESENTS THE RESULTS OF large eddy simulation/conditional moment closure (LES-CMC) computations of a turbulent flame in oxy-combustion regimes complemented by 0D-CMC analysis. The fuel is pure hydrogen and it issues into a hot oxidiser stream which is a mixture of oxygen and water vapour. The flame is initiated by a spark, then it spreads and propagates through the domain and eventually stabilises as a lifted or attached one. The present problem offers new challenges to combustion modelling as the observed combustion process is strongly unsteady. In cases of large content of oxygen in the oxidiser stream the flame has very high temperature (≈ 3000 K) and large temperature/density variations. Nevertheless, it is shown that LES-CMC simulations are stable in such conditions and can be successfully applied to oxy-combustion studies. We analyse the dependence of the flame temperatures and lift-off height of the flames L_H on the oxidiser composition and chemical kinetics. It is shown that both these factors may affect the flame behaviour. We identified the conditions in which L_H exhibits a linear dependence on the oxidiser composition independently of applied chemical kinetics, and the regimes where the L_H changes in a non-linear manner and strongly depends on the chemical kinetics.

Key words: LES, CMC, turbulent lifted flame, clean combustion.

Copyright © 2017 by IPPT PAN

1. Introduction

OXY-COMBUSTION TECHNOLOGY WAS PROPOSED INDEPENDENTLY BY HORN and STEINBERG [1] and ABRAHAM *et al.* [2] in the 1980s as a tool reducing pollutant emission of greenhouse gases. In oxy-combustion processes an oxidiser stream is modified in such a way that the nitrogen present in the air is replaced by recycled (or inert) gas and thus the NO_x formation can be reduced. This technology is currently in the developing stage and many questions related to combustion characteristics, ignition, flame stability or optimal oxidiser composition remain unanswered. Although, in principle, the oxy-combustion technology

*The author previous surname was Rosiak, changed to Wawrzak after marriage.

can be applied to every type of fuel, the majority of research in this field concentrates mainly on oxy-coal and oxy-natural gas combustion [3] as they are the most abundant fuels. However, the use of these fuels does not eliminate the emission of CO₂ to the atmosphere, which taking into account current discussions on global warming, is of the same importance as the NO_x emission. A possible solution to this problem is to use the hydrogen fuel, which in a combination with an oxidiser not containing compounds leading to CO₂ and NO_x formation would result in clean combustion products. The present study is focused on numerical modelling of non-premixed combustion of pure hydrogen and as a model problem we consider a jet issuing into a co-flowing stream being a mixture of the oxygen and water vapour at various proportions. With such a fuel/oxidiser composition, assuming that the combustion process is complete, the only combustion products are the water vapour and residues of oxygen. Thus, we may say that we achieve a perfectly clean combustion free of any pollutants. The approach presented in the present work is of a pioneering character, which besides the application of a complex numerical method for the analysis of strongly unsteady phenomena (ignition, flame propagation) in oxy-combustion regimes, also shows that existing configurations can be successfully adapted for such study. We analyse the well-known configuration of CABRA *et al.* [4] in which we modified the fuel and oxidiser composition by replacing the nitrogen with the water vapour. Hence, in addition to a huge interest in the field of oxy-combustion technology, the present work may turn out worthwhile considering a possibility of future use of old set-ups for new research.

Experimental and numerical studies on the influence of addition of the water vapour to a fuel/oxidiser mixture on ignition and extinction phenomena in premixed and non-premixed systems (counterflow configuration) were performed by SEISER and SESHADRI [5]. They showed that addition of the water vapour with the mass fraction $Y_{\text{H}_2\text{O}} \leq 0.2$ made the flames harder to ignite and easier to extinguish. Similarly, in the recent research devoted to auto-ignition of hydrogen jet in O₂/H₂O atmosphere [6] it was found that the auto-ignition had occurred when $Y_{\text{H}_2\text{O}} \leq 0.5$ in the oxidiser stream. Additionally, an interesting finding was that the flame lift-off height appeared only slightly sensitive to the oxidiser temperature. Such a flame behaviour was attributed to the fact that in those studies the excess of O₂ related to H₂ was kept constant and this assumption required changing the oxidiser velocity. It seems that these modifications restrained the importance of the oxidiser composition and its temperature. These observations became the motivation for the present study in which we assume a constant oxidiser velocity and we focus on dependence of the flame position and its temperature on the oxidiser composition and method of modelling of chemical reactions. We compare the results obtained using two chemical kinetics, which were previously proven to work well for the hydrogen combustion

in the air, i.e., we consider the chemical mechanisms formulated by MUELLER *et al.* [7] and LI *et al.* [8]. The present research has an exploratory character as there is no experiment available for oxy-combustion of pure hydrogen jet and to the best knowledge of the authors no numerical study of such a configuration has been performed before.

We use one of the most advanced and accurate numerical combustion models, i.e., conditional moment closure (CMC) combined with large eddy simulation (LES) method. In oxy-combustion studies, the LES method in connection with the EDC model was used recently by WARZECHA and BOGUSLAWSKI [9, 10] for the analysis of pulverised coal combustion. PEDEL *et al.* [11] also used the LES method for the analysis of an auto-ignition mechanism, stability and flame lift-off in a co-axial jet (pulverized coal/O₂/CO₂) while studying the experimental configuration used in [12]. In combination with the CMC approach the LES was used by GARMORY and MASTORAKOS [13] for modelling a combustion of CH₄/H₂ in O₂/CO₂ atmosphere and it turned out to be able to predict extinction and flame lift-off phenomena.

2. Modelling

LES-CMC method is increasingly being used for challenging combustion phenomena, including modelling of lifted flames [14], local extinctions [15], auto-ignition [16, 17] or forced ignition [18]. In present study we use a LES-CMC code thoroughly validated in both non-reacting flows as well as in combustion problems including Sandia flames, the Cabra flame and flame/flow control issues, see [19–21] and papers cited there. Though there are not exemplary data available for verification purposes it is believed that the applied code will provide the results as accurate as in the previous studies. To ensure that, in this work we adapt an already studied configuration of well known Cabra flame [4] in which we modified the composition of fuel and oxidiser (see Sec. 3).

2.1. LES model

In LES the flow scales are divided into large scales, directly solved on a given numerical mesh, and small scales (the so-called sub-grid or sub-filter scales) which require modelling. The scale separation is obtained by a spatial filtering defined as [22, 23]: $\bar{f}(\vec{x}, t) = \int_{\Omega} G(\vec{x} - \vec{x}', \Delta) f(\vec{x}', t) d\vec{x}'$, where f stands for arbitrary variable and $G(x, \Delta)$ is filter function. Its filter width is equal to $\Delta = Vol^{1/3}$, where Vol stands for a local mesh volume. In the variable density flows the Favre filtering is applied with the filtered variables expressed as $\tilde{f}(\vec{x}, t) = \overline{\rho f} / \bar{\rho}$, where ρ is the density. Applying the filtering procedure to the continuity and

the Navier–Stokes equations gives:

$$(2.1) \quad \frac{\partial \bar{\rho}}{\partial t} + \frac{\partial \bar{\rho} \tilde{u}_j}{\partial x_j} = 0,$$

$$(2.2) \quad \frac{\partial \bar{\rho} \tilde{u}_i}{\partial t} + \frac{\partial \bar{\rho} \tilde{u}_i \tilde{u}_j}{\partial x_j} = -\frac{\partial \bar{p}}{\partial x_i} + \frac{\partial \tau_{ij}}{\partial x_j} + \frac{\partial \tau_{ij}^{sgs}}{\partial x_j},$$

where u_i are the velocity components, p is the pressure, τ_{ij} and τ_{ij}^{sgs} are the stress tensors of the resolved and unresolved (sub-grid) velocity field. The first one is defined as $\tau_{ij} = \mu [2S_{ij} - \frac{2}{3}\delta_{ij}\partial\tilde{u}_k/\partial x_k]$, and the latter is modelled by an eddy viscosity type model [23] as: $\tau_{ij}^{sgs} = 2\mu_t S_{ij} - \tau_{kk}\delta_{ij}/3$, where $S_{ij} = \frac{1}{2}(\partial\tilde{u}_i/\partial x_j + \partial\tilde{u}_j/\partial x_i)$. The variable μ_t is the sub-grid viscosity which in the present work is computed according to the model proposed by VREMAN [24].

2.2. LES-CMC formulation

The CMC model has been formulated in the 1990s by KLIMENKO and BILGER [25], it belongs to the family of the mixture fraction-based models [26]. The mixture fraction ξ is the variable which represents the local fuel/oxidiser ratio. It varies in the range $0 \leq \xi \leq 1$, i.e., $\xi = 0$ denotes oxidiser stream and $\xi = 1$ corresponds to the fuel stream. The mixture fraction is a conserved quantity and it obeys the classical convection-diffusion transport equation, which in the framework of LES is defined as

$$(2.3) \quad \frac{\partial \bar{\rho} \tilde{\xi}}{\partial t} + \frac{\partial \bar{\rho} \tilde{u}_i \tilde{\xi}}{\partial x_i} = \frac{\partial}{\partial x_i} \left(\bar{\rho} (\mathcal{D} + \mathcal{D}_t) \frac{\partial \tilde{\xi}}{\partial x_i} \right),$$

where $\mathcal{D} = \mu/\bar{\rho}Sc$ and $\mathcal{D}_t = \mu_t/\bar{\rho}Sc_t$ are the molecular and sub-grid diffusivities, and $Sc = Sc_t = 0.7$ are the Schmidt numbers [27]. The CMC model, in the context of LES, has been developed in [28] based on the density-weighted conditional filtering operation applied to the transport equations for the species mass fraction (Y_k) and total enthalpy (h). The conditionally filtered species mass fractions will be denoted as: $Q_k = Y_k|\eta$, where $k = 1, \dots, n$, is the index of n reacting species, and $Q_h = \tilde{h}|\eta$ will stand for the conditionally filtered enthalpy. The variable η is the sample space for ξ and the operator $(\cdot|\eta)$ is the conditional filtering operator with conditioning being done on ξ [27, 28]. The conditionally filtered variables are related to the filtered variables by the integration over the η space as:

$$(2.4) \quad \tilde{f}(\vec{x}, t) = \int_0^1 f|\eta \tilde{P}(\vec{x}, t, \eta) d\eta,$$

where \tilde{P} is a filtered probability density function assumed here as a beta-function PDF defined as [29]

$$(2.5) \quad P(\eta) = \eta^{a-1}(1-\eta)^{b-1} \frac{\Gamma(a+b)}{\Gamma(a)\Gamma(b)},$$

parametrized by $\tilde{\xi}$ and its variance $\tilde{\xi}''^2$ through the variables:

$$a = \tilde{\xi}(\tilde{\xi}(1-\tilde{\xi})/\tilde{\xi}''^2 - 1) \quad \text{and} \quad b = a(1-\tilde{\xi})/\tilde{\xi}.$$

The variance $\tilde{\xi}''^2$ is modelled as $\tilde{\xi}''^2 = C_V \Delta^2 \frac{\partial \tilde{\xi}}{\partial x_j} \frac{\partial \tilde{\xi}}{\partial x_j}$ with the constant $C_V = 0.1$, as suggested in [30]. The symbol $\Gamma(x)$ in Eq. (2.5) is the gamma function. Applying the conditional filtering procedure to the transport equations for species mass fraction and enthalpy leads to the CMC equations given as [27, 28]:

$$(2.6) \quad \frac{\partial Q_k}{\partial t} + \widetilde{u_i|\eta} \frac{\partial Q_k}{\partial x_i} = \widetilde{N|\eta} \frac{\partial^2 Q_k}{\partial \eta^2} + \widetilde{\dot{\omega}_k|\eta} + e_Y,$$

$$(2.7) \quad \frac{\partial Q_h}{\partial t} + \widetilde{u_i|\eta} \frac{\partial Q_h}{\partial x_i} = \widetilde{N|\eta} \frac{\partial^2 Q_h}{\partial \eta^2} + e_h.$$

The first terms on the right-hand side of Eqs. (2.6) and (2.7) represent the diffusion in mixture fraction space. The last terms on the right hand side, i.e., e_Y, e_h , represent the sub-grid interactions and they are usually expressed as [14, 16, 27]:

$$e_Y = \frac{\partial}{\partial x_i} \left(\widetilde{\mathcal{D}_t|\eta} \frac{\partial Q_k}{\partial x_i} \right), \quad e_h = \frac{\partial}{\partial x_i} \left(\widetilde{\mathcal{D}_t|\eta} \frac{\partial Q_h}{\partial x_i} \right),$$

where $\widetilde{\mathcal{D}_t|\eta}$ is the conditionally filtered subgrid diffusivity assumed to be uniform in η -space and modelled as $\widetilde{\mathcal{D}_t|\eta} \approx \mathcal{D}_t$ [27]. The same assumptions are made concerning the conditionally filtered velocity, i.e., $\widetilde{u_j|\eta} \approx \tilde{u}_j$ [27]. The conditionally filtered reaction rate is evaluated with the first order closure [25] where the sub-grid conditional fluctuations are neglected, i.e., $\widetilde{\dot{\omega}_k|\eta} = \dot{\omega}_k(Q_1, Q_2, \dots, Q_n, Q_h)$. The conditional scalar dissipation rate $\widetilde{N|\eta}$ is modelled applying the amplitude mapping closure (AMC) model [31, 32] defined as:

$$(2.8) \quad \begin{aligned} \widetilde{N|\eta} &= N_0 G(\eta), \\ G(\eta) &= \exp(-2[\text{erf}^{-1}(2\eta-1)]^2), \\ N_0 &= \frac{\tilde{N}}{\int_0^1 G(\eta) \tilde{P}(\eta) d\eta}, \end{aligned}$$

where $\text{erf}(x)$ is the error function. The filtered scalar dissipation rate \tilde{N} is computed as the sum of the resolved and subgrid part [27, 28]:

$$(2.9) \quad \tilde{N} = \underbrace{\mathcal{D} \left[\frac{\partial \tilde{\xi}}{\partial x_i} \frac{\partial \tilde{\xi}}{\partial x_i} \right]}_{\text{resolved}} + \underbrace{\frac{1}{2} C_N \frac{\nu_t}{\Delta^2} \tilde{\xi}''^2}_{\text{subgrid}},$$

where the model constant C_N in Eq. (2.9) is set $C_N = 42$ following the analysis presented in [15], based on the calibration for Sandia F flame, and in [33] based on the computations for two-phase flows.

As the CMC model is defined in the four-dimensional space (physical space \vec{x} and η -space) its application is very expensive computationally. A typical approach reducing the computational costs is based on the use of two separate meshes in physical space, i.e., one for the flow field (called CFD mesh), and the second, much coarser, for the CMC equations (called CMC mesh). Various possibilities to transfer the variables ($\tilde{N}|\eta$, $\tilde{u}|\eta$, $\tilde{\mathcal{D}}_t|\eta$) from the CFD to CMC mesh have been discussed in [27]. One of the analysed approaches, adapted in the present work, was to compute the conditional variables on the CMC mesh (denoted generally as $\tilde{f}|\eta^*$) as the mass weighted volume integral within the CMC cells (V_{CMC}). This is defined as: $\tilde{f}|\eta^* = \int_{V_{CMC}} \tilde{\rho} \tilde{P}(\eta) \tilde{f}|\eta dV' / \int_{V_{CMC}} \tilde{\rho} \tilde{P}(\eta) dV'$. Thus, the conditionally filtered variable $\tilde{f}|\eta^*$ corresponding to the CMC cell is common for a group of the CFD nodes embedded in that CMC cell. The solution of CMC equations provides Q_k^* and Q_h^* on the CMC mesh. Then, the resolved variables are computed as $\tilde{Y}_k(\vec{x}, t) = \int_0^1 Q_k^* \tilde{P}(\vec{x}, t, \eta) d\eta$ and $\tilde{h}(\vec{x}, t) = \int_0^1 Q_h^* \tilde{P}(\vec{x}, t, \eta) d\eta$.

2.3. Numerical methods

The computations are performed using an in-house high-order LES solver based on the low Mach number approach. The spatial discretisation is performed on half-staggered meshes [34, 35] by the sixth-order compact method for the Navier–Stokes and continuity equations and with fifth-order WENO scheme for the mixture fraction. The time integration is performed with a predictor-corrector approach with the second-order Adams–Bashforth and Adams–Moulton methods.

The CMC equations are solved by applying the operator splitting approach where the transport in physical space, transport in mixture fraction space and chemistry are solved separately. Time integration in physical space is performed with the first-order explicit Euler method. The CMC terms in physical space are discretised with second-order methods. The convective terms were discretised using second-order TVD method with van Leer’s limiters. In mixture fraction space the CMC equations are stiff due to the reaction rate terms. In this case, the time integration had to be performed applying the VODPK package (a variable-

coefficient ordinary differential equation solver with the preconditioned Krylov method GMRES for the solution of linear systems) [36–38]. The CMC terms in mixture fraction space are discretised using the second-order finite difference method. The reaction rates are computed using a CHEMKIN interpreter. In the chemical mechanism proposed by MUELLER *et al.* [7] there are 9 species/21 reactions and in that proposed by LI *et al.* [8] we have 13 species/25 reactions.

3. Simulation details

3.1. Problem description

As there are no experimental data available for combustion of pure H₂ jet in the mixture of O₂/H₂O in the present work we adapted a configuration used by CABRA *et al.* [4] for the auto-ignition studies of turbulent H₂/N₂ jet in a co-flow of hot combustion products of lean H₂/air flame. This choice is motivated by the fact that for this test case the LES-CMC results obtained by many researchers (including the authors [17]) were in good agreement with the experimental findings. In the present case, the fuel is replaced by the pure hydrogen and the co-flow is the mixture of oxygen and water vapour. The computational configuration is shown schematically in Fig. 1. The fuel jet is injected through a nozzle with the internal diameter $D = 0.00457$ m at the ambient pressure. The fuel temperature and bulk velocity are equal to $T_F = 305$ K and $U_F = 107$ m/s, respectively. The velocity across the pipe is assumed as a fully developed flow and calculated using the 1/7 law. We consider various oxidiser compositions with the mass fraction of water vapour varying in the range of $Y_{H_2O} = 0.2 - 0.9$. Assuming that the oxygen mass fraction is computed as $Y_{O_2} = 1 - Y_{H_2O}$ in the following discussions we will refer to Y_{H_2O} only. Preliminary results [6] obtained with two co-flow temperatures $T_{CF} = 1030$ K, $T_{CF} = 1045$ K performed for a 30% excess of mass flow rate of O₂ relative to H₂ showed that in comparison to the co-flow temperatures the velocity of the co-flow has much more impact on the results. In the present study we assume the co-flow temperature $T_{CF} = 1045$ K and velocity $U_{CF} = 16.48$ m/s, which in [6] has led to a large lift-off height (L_H in Fig. 1). We analyse how L_H changes with the oxidiser composition and chemical kinetics.

Table 1. Stoichiometric mixture fraction and the most reactive mixture fraction computed using the chemical kinetics of MUELLER *et al.* [7] and LI *et al.* [8].

Mixt. fract./ $Y_{H_2O} \rightarrow$	0.2	0.3	0.4	0.5	0.6	0.7	0.8	0.85	0.9
ξ_{ST}	0.0916	0.0811	0.0703	0.0593	0.0480	0.0364	0.0246	0.0185	0.0124
$\xi_{MR} \times 10^{-3}$ [7]	1.40	2.30	2.90	3.30	3.76	4.31	4.70	5.11	5.46
$\xi_{MR} \times 10^{-3}$ [8]	1.10	2.00	2.60	3.00	3.51	3.88	4.32	4.58	4.97

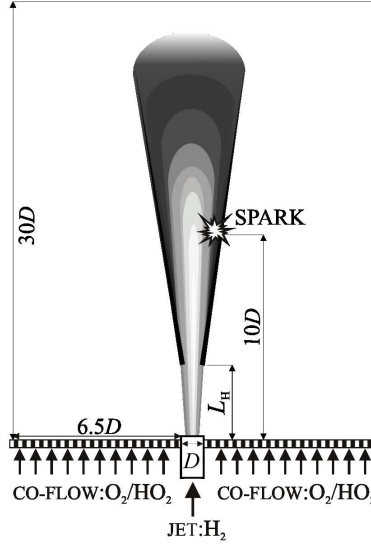


FIG. 1. Schematic view of the analysed configuration.

3.2. Computational domain

The computational domain is a rectangular box with dimensions $L_x \times L_y \times L_z = 14D \times 30D \times 14D$, where the y coordinates the stream axis. The four dimensional (x, y, z, η) solution space assumed in the LES-CMC approach implies very large computational costs related to the need of solutions of the CMC equations in mixture fraction space in every physical grid node. As mentioned in Sec. 2.2, a common simplifying approach relies on the application of two separate meshes, i.e., one for the solution of the flow field and second (much coarser) for the CMC equations. In this work, the CFD mesh consists of $128 \times 160 \times 128$ nodes stretched radially and axially towards the jet region and the CMC mesh is uniform and composed of $15 \times 80 \times 15$ nodes. The mesh in mixture fraction space consisted of 51 nodes compacted near the stoichiometric value. Influence of the mesh density was examined in preliminary computations and also in a previous study related to the original Cabra flame configuration [17]. It was found that minor differences did not change the main features of the flames.

4. Results

4.1. 0D-CMC analysis in mixture fraction space

LES-CMC simulations are preceded by the so-called 0D-CMC calculations performed using the 0D-CMC model, which corresponds to Eqs. (2.6)–(2.7)

without the transport terms in physical space. In such simulations the values of $\widetilde{N|\eta}$ are obtained for an *a priori* assumed maximum scalar dissipation rate $N_0 = 1, 10, 100, 1000 \text{ s}^{-1}$ used in the AMC model (see Eq. (2.8)).

Although the obtained 0D solutions concern mixture fraction space only, they give insight on how the oxidiser parameters affect the maximum flame temperature ($T|\eta_{\max}$), auto-ignition time (t_{ign}) or species composition. Table 1 reports dependence of the stoichiometric mixture fraction (ξ_{ST}) and the so-called the most reactive mixture fraction (ξ_{MR}) on oxidiser compositions for both chemical mechanisms. The values of ξ_{ST} decrease almost linearly with an increasing $Y_{\text{H}_2\text{O}}$, while ξ_{MR} shows the opposite trend. The ξ_{MR} depends on chemistry only slightly but it is worth noting that in the whole range of $Y_{\text{H}_2\text{O}}$ the ξ_{MR} is smaller in the chemical mechanism of Li *et al.* [8].

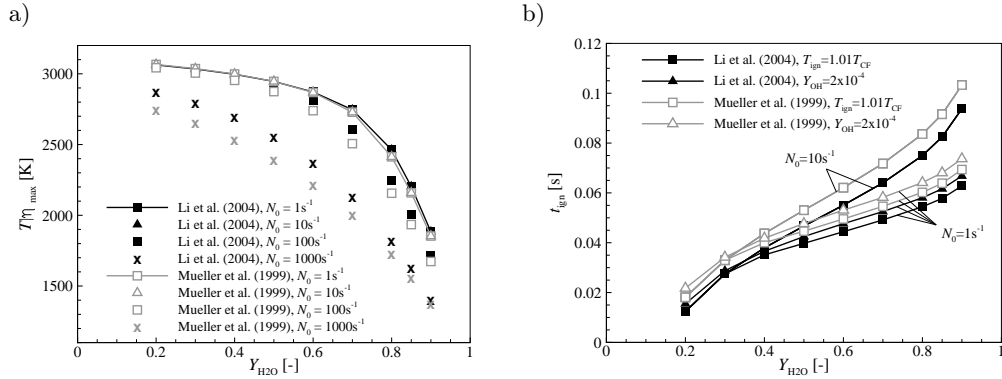


FIG. 2. Dependence of (a) $T|\eta_{\max}$ and (b) t_{ign} on $Y_{\text{H}_2\text{O}}$ for 0D-CMC.

Dependence of the maximum temperature and auto-ignition time on $Y_{\text{H}_2\text{O}}$ and N_0 is shown in Fig. 2. As t_{ign} we consider the time moment in which the temperature rises 1% over the T_{CF} or when Y_{OH} reaches 2×10^{-4} . The evolution of $T|\eta_{\max}$ was obtained from the computations performed such that starting from the “burning solution” for $N_0 = 1 \text{ s}^{-1}$ the value of N_0 was successively increased and the calculations continued until the difference between $T|\eta_{\max}$ in two successive time steps was smaller than 10^{-4} K . As N_0 changes the strengths of diffusion in mixture fraction space and $Y_{\text{H}_2\text{O}}$ affects the boundary conditions and determines the amount of water vapour and oxygen in the oxidiser stream (i.e., at $\eta = 0$), it can be seen in Fig. 2a that $T|\eta_{\max}$ largely depends on both these parameters and decreases as they increase. Differences between $T|\eta_{\max}$ obtained with two chemical mechanisms for $N_0 = 1 \text{ s}^{-1}$ and $N_0 = 10 \text{ s}^{-1}$ are not large. For $N_0 = 10^2 \text{ s}^{-1}$ and $N_0 = 10^3 \text{ s}^{-1}$ the differences are much more pronounced, but it should be noted that they decrease for large $Y_{\text{H}_2\text{O}}$.

Analysis of the auto-ignition process consisted in the simulations which begun from assumed inert solutions and were continued until the auto-ignition has occurred and the steady state has been reached. As the successful auto-ignition we understand the case in which after a rise of temperature the solution converges to the same state as if it was initialized with a “burning solution”. For $N_0 = 1 \text{ s}^{-1}$, 10 s^{-1} this happens for the entire range of $Y_{\text{H}_2\text{O}}$, and for $N_0 = 10^2 \text{ s}^{-1}$ only for $Y_{\text{H}_2\text{O}} = 0.2$, while for $N_0 = 10^3 \text{ s}^{-1}$ the auto-ignition does not occur at all. In these cases the temperature rises very little and does not increase. As can be seen in Fig. 2b, for the oxidiser compositions rich in the oxygen (i.e., for $Y_{\text{H}_2\text{O}} \leq 0.3$) t_{ign} is very short and virtually independent of N_0 . Substantial differences appear when $Y_{\text{H}_2\text{O}}$ increases and for $Y_{\text{H}_2\text{O}} = 0.9$ they reach $\Delta t_{\text{ign}} = 3 \times 10^{-2} \text{ s}$.

It can be seen in Fig. 2b that the auto-ignition criterion $T_{\text{ign}} = 1.01T_{\text{CF}}$ predicts t_{ign} to be slightly shorter than when using the condition $Y_{\text{OH}} = 2 \times 10^{-4}$, however, the trends of t_{ign} are similar in both the cases. The same can be said concerning t_{ign} calculated using different chemical kinetics. In this case the observed differences are of the same order as in the case of using different auto-ignition criterion. It can be seen that the chemical mechanism of LI *et al.* [8] shows t_{ign} shorter by $\Delta t_{\text{ign}} = 5 - 8 \times 10^{-3} \text{ s}$. Although this might seem small it may turn out important regarding the lift-off height of the flame. One could intuitively assume that a fuel/oxidiser interface “travels” axially with a mean convection velocity estimated as $U_m \propto (U_F + U_{\text{CF}})$. The chemical reactions hold and the chemical source terms compete with the diffusion and convection transport terms. When the former exceed the latter the ignition occurs and the chemical and transport forces equalise at L_H . Assuming that the duration of the above “travelling process” is proportional to t_{ign} one can roughly estimate that $L_H \propto U_m t_{\text{ign}}$, which would mean that a shorter t_{ign} leads to a smaller L_H .

4.2. LES-CMC unsteady results

The LES-CMC simulations started from the quiescent conditions in the whole domain. The fuel and co-flow air are injected impulsively and flow through the domain. After a while, when the jet fully develops the flame is initiated by a “numerical spark” which in mixture fraction space corresponded to the solution obtained in 0D-CMC simulation. Such a spark was imposed for a time $t_{\text{spark}} = 1 \text{ ms}$ in the CMC cells belonging to a volume V_{spark} with the diameter of 5 mm. In this paper, we are not interested in analysis of success or failure of the ignition events and therefore we placed the spark in the region of very high ignition probability, i.e., in the shear layer [39]. The process of ignition, flame development and stabilisation for the case with $Y_{\text{H}_2\text{O}} = 0.6$ computed by using the mechanism of MUELLER *et al.* [7] is presented in the Fig. 3 showing contours

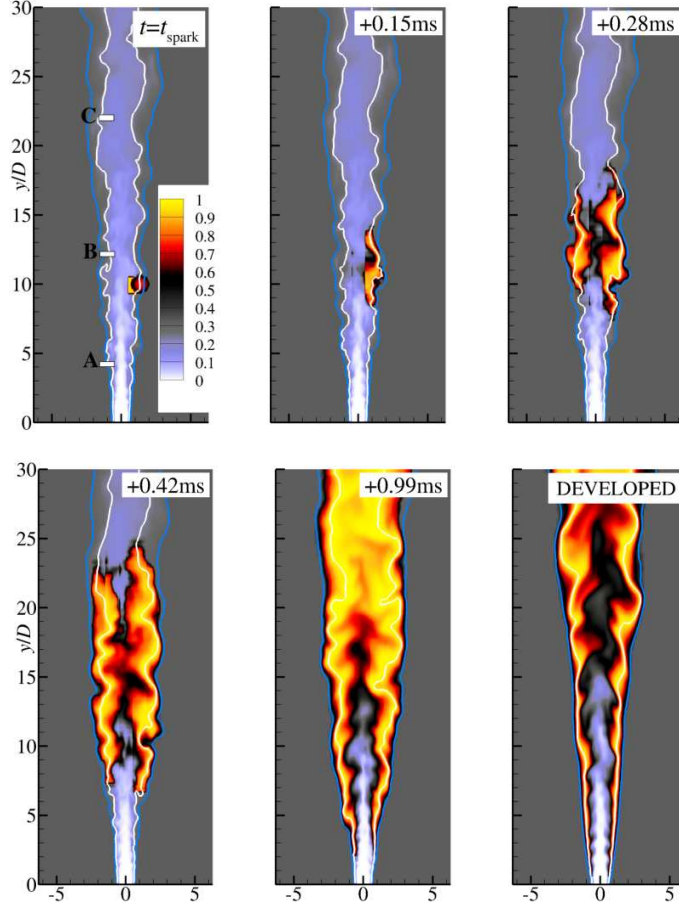


FIG. 3. Evolution of normalised temperature $\tilde{T}/T|\eta_{\max}$ during the spark ignition and flame development phases for $Y_{\text{H}_2\text{O}} = 0.6$. The white and blue lines denote $\xi_{\text{ST}} = 4.8 \times 10^{-2}$ and $\xi_{\text{MR}} = 3.76 \times 10^{-3}$.

of the temperature normalised by $T|\eta_{\max}$ obtained for $Y_{\text{H}_2\text{O}} = 0.6$. The white and blue lines denote localisation of $\xi_{\text{ST}} = 4.8 \times 10^{-2}$ and $\xi_{\text{MR}} = 3.76 \times 10^{-3}$, respectively. In the contour plots we use the normalised values of the temperature as those obtained directly from the LES-CMC solutions differ very significantly depending on $Y_{\text{H}_2\text{O}}$. They would not be readable when shown in a common scale covering whole range. It can be seen in Fig. 3 that after the spark has been switched-off the flame propagates very quickly and achieves the fully developed state in approximately 10^{-2} s. A qualitatively similar spark-ignition scenario can be observed for the case with $Y_{\text{H}_2\text{O}} = 0.85$ presented in Fig. 4, though, in this case the flame stabilises in a lifted position. Analysis of the temperature field reveals that compared to the case with $Y_{\text{H}_2\text{O}} = 0.6$ in the present situation with the

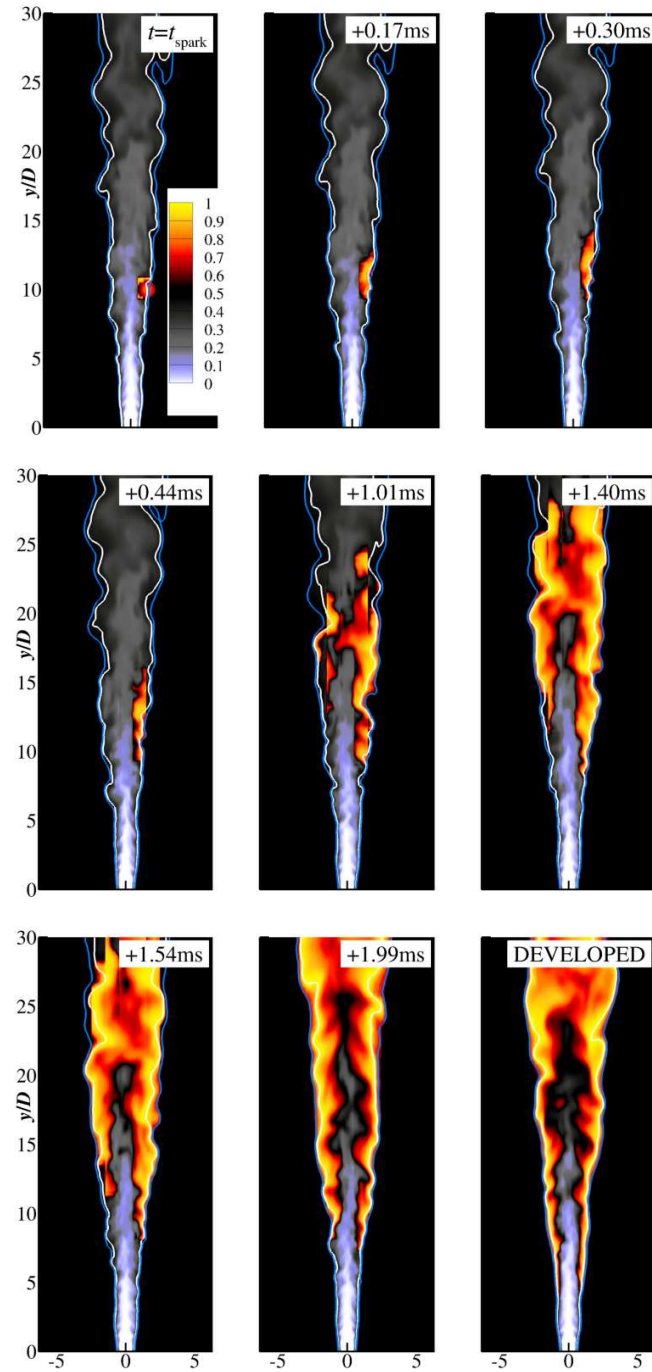


FIG. 4. Evolution of normalised temperature $\tilde{T}/T|_{\eta_{\max}}$ during the spark ignition and flame development phases for $Y_{\text{H}_2\text{O}} = 0.85$. The white and blue lines denote $\xi_{\text{ST}} = 1.85 \times 10^{-2}$ and $\xi_{\text{MR}} = 5.11 \times 10^{-3}$.

larger amount of the water vapour in the oxidiser the ignition process is inhibited and the propagation phase is slowed down (cf. Fig. 3). It can be noticed that at the similar time instances of the ignition the flames obtained for $Y_{\text{H}_2\text{O}} = 0.6$ and $Y_{\text{H}_2\text{O}} = 0.8$ are anchored at different positions from the inlet, their sizes are significantly different and eventually they stabilise as attached or lifted.

The processes of flame initiation and propagation are always regarded as strongly unsteady, and as such, very difficult to predict in numerical simulations. Nevertheless, it seems that in the present case they are well captured by the LES-CMC, at least qualitatively. It is seen that the flame propagates first along the ξ_{ST} line and then radially. It spreads faster towards the downstream region, where the fuel/oxidiser mixing intensity is high and the scalar dissipation rate is low, than towards the upstream part. This behaviour is typically observed in jet type flames. The propagation of the flame in physical space is connected with its development in mixture fraction space as “burning CMC” cells affect neighbouring “cold CMC” cells through the convection and diffusion mechanisms. Figure 5 shows the time evolution of $T|\eta$ in the CMC cells A, B and C shown in

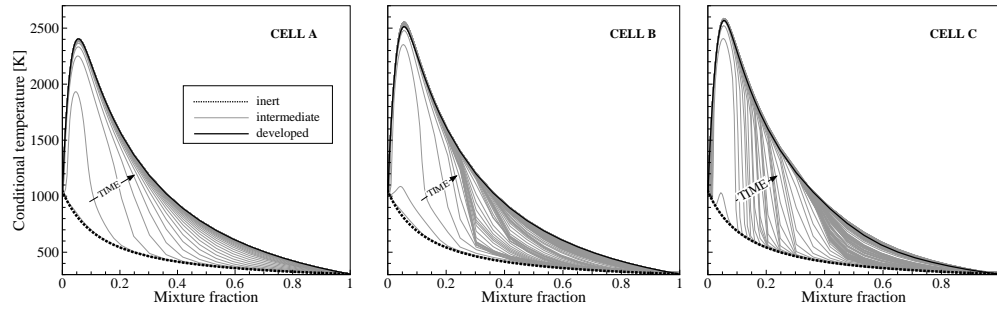


FIG. 5. Time variation of $T|\eta$ in the CMC cells A, B and C for $Y_{\text{H}_2\text{O}} = 0.6$.

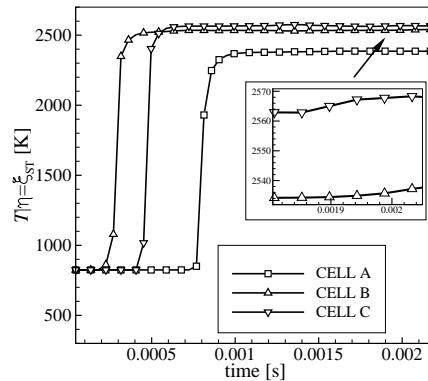


FIG. 6. Time variation of $T|\eta = \xi_{\text{ST}}$ in the CMC cells A, B and C for $Y_{\text{H}_2\text{O}} = 0.6$.

Fig. 3. The black dotted lines correspond to the time instances when the flame is far from the particular cells. The intermediate state when the flame approaches and passes through the CMC cells is represented by the thin grey lines, each representing the solution every 4.52×10^{-5} s. The solid black lines correspond to the fully developed conditions. Although this state differs depending on the spatial location its time variation is very small. Similar analysis performed for different CMC cells, for different $Y_{\text{H}_2\text{O}}$ and also for the species (e.g., $Y_{\text{OH}}|\eta$, $Y_{\text{HO}_2}|\eta$) exhibits very similar behaviour meaning that in the analysed flames the solutions in mixture fraction space are almost stationary. This is illustrated in Fig. 6 showing the time variations of $T|\eta = \xi_{\text{ST}}$ in the cells A, B and C. Sudden temperature rises are related to passing the flame front through the CMC cells. It can be seen that after that moment the temperature oscillations are very small.

4.3. LES-CMC time-averaged results

Time-averaging procedure started from the fully developed flames and lasted for 3.57×10^{-2} s, which based on the co-flow velocity is equivalent to approximately 4.6 flows through time. Sample results showing the contours of time-averaged temperature are shown in Fig. 7, where it can be seen that L_{H} strongly depends on $Y_{\text{H}_2\text{O}}$. A close inspection of the regions near the points in which the flames are stabilised, shows that at these locations the iso-lines ξ_{ST} and ξ_{MR} , which are initially (i.e., for $y/D < L_{\text{H}}$) nearly parallel and close to each other, start to diverge. It can be seen that the radial distance between ξ_{ST} and ξ_{MR} increases with y/D distance, but it decreases as $Y_{\text{H}_2\text{O}}$ increases.

Figure 8 shows a dependence of L_{H} on $Y_{\text{H}_2\text{O}}$, the chemical kinetics and the criterion of determining of L_{H} . It is seen that the last parameter, unlike in the 0D-CMC analysis of the auto-ignition, practically plays no role and tiny differences are noticed only for large L_{H} . The chemical kinetics seems much more important in this figure. For $Y_{\text{H}_2\text{O}} \leq 0.6$ the L_{H} is virtually the same for both schemes and exhibits a linear behaviour. For $Y_{\text{H}_2\text{O}} > 0.6$ it grows in a strongly non-linear manner and differences between the applied chemistry become readily apparent. For $Y_{\text{H}_2\text{O}} = 0.85$ the chemical mechanism of LI *et al.* [8] predicts L_{H} to be twice longer. This is in contradiction to the discussion in the last paragraph in Sec. 4.1 according to which the shorter auto-ignition time determined by 0D-CMC in the mechanism of LI *et al.* [8] should lead to a shorter L_{H} . The LES-CMC revealed the opposite behaviour and suggested that the assumptions concerning importance of t_{ign} were exaggerated and needed rethinking. Indeed, a close analysis of the flow fields showed that the velocity in the region upstream of the ignition point (flame stabilisation point) in the case of the simulations performed using the mechanism of LI *et al.* [8] is, depending on $Y_{\text{H}_2\text{O}}$, approximately 1.0–1.5 m/s larger compared to the solutions obtained

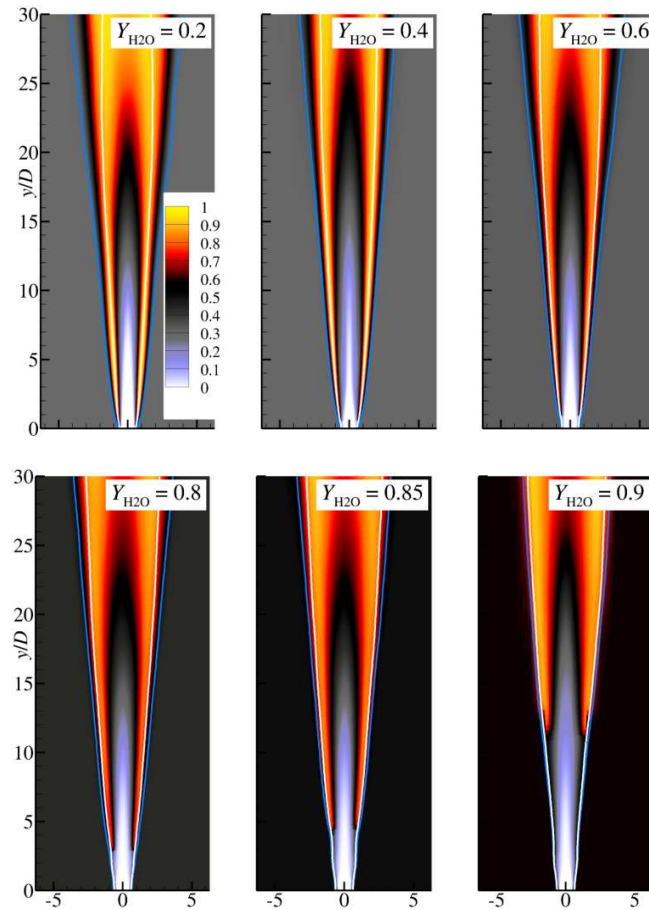


FIG. 7. Contours of the normalised time-averaged temperature $\langle \tilde{T} \rangle / T|_{\eta_{\max}}$ obtained with the chemical mechanism of MUELLER *et al.* [7].

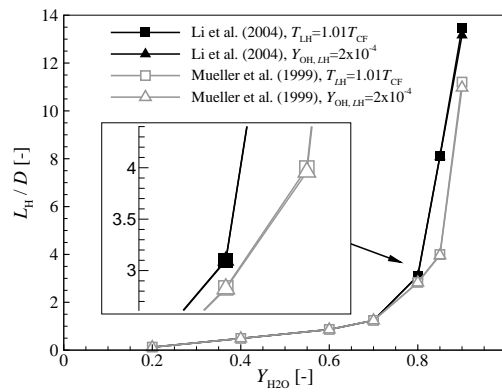


FIG. 8. Lift-off height as a function of Y_{H_2O} .

with the mechanism of MUELLER *et al.* [7]. The larger velocity results from a slightly different (smaller) density of the mixture upstream the of ignition point, which is caused by different chemistry condition. In effect, the larger jet velocity shifts the ignition point further downstream from the inlet and this behaviour is consistent with the literature [40].

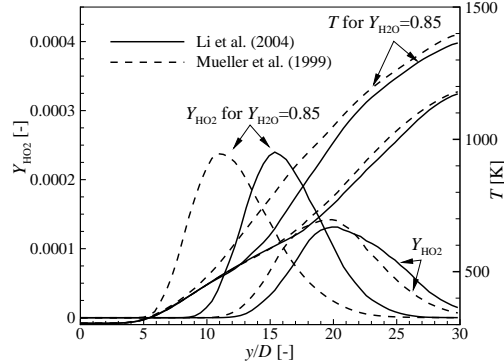


FIG. 9. Axial profiles of \tilde{Y}_{HO_2} and \tilde{T} .

The axial distribution of temperature and the mass fraction of the so-called pre-ignition species HO_2 are shown in Fig. 9. It can be seen that for $Y_{\text{H}_2\text{O}} = 0.85$ differences between the particular schemes are very significant, whereas for $Y_{\text{H}_2\text{O}}$ larger and smaller than 0.85 (not shown) the solutions become similar. This suggests that the analysed case is sensitive to chemical kinetics only in some range of $Y_{\text{H}_2\text{O}}$, but this statement requires further studies for different co-flow temperature and velocity.

5. Conclusions

The LES-CMC approach was applied to the combustion modelling of hydrogen jet issuing into a co-flow of hot $\text{O}_2/\text{H}_2\text{O}$ mixture. To the best authors' knowledge this research constitutes one of the first attempts of perfectly clean combustion in the field of LES-CMC modelling. The LES-CMC modelling proved to be very useful in such studies and enabled analysis of complete combustion process from ignition to flame stabilisation. The obtained results showed very large impact of the co-flow composition on the maximum flame temperatures and lift-off heights. It was shown that they can be effectively controlled in a very wide range ($\tilde{T}_{\text{max}} \approx 1700 \text{ K} \rightarrow 3000 \text{ K}$, $L_{\text{H}}/D = 0 \rightarrow 13$) by changing the amount of H_2O in the oxidiser. An important and somewhat surprising finding of this study is the fact that for some range of H_2O in the oxidiser L_{H} significantly depended on the chemical kinetics. Furthermore, the observed dependence

showed an opposite trend than expected from the 0D-CMC simulations. Such a behaviour of the flame in the 3D LES-CMC simulations has been attributed to the occurrence of small differences in the velocity and density fields upstream of the ignition points. Hence, one may conclude that in the analysed configuration there is a range of oxidiser compositions for which the differences in the flow field affect the flame more than one could presume based on the simplified analyses. Certainly, this aspect requires further parametric studies involving additional chemical mechanisms and/or more advanced combustion modelling, e.g., taking into account a possible influence of differential diffusion, which in the present studies was completely neglected.

Acknowledgements

This work was supported by grant 2014/13/B/ST8/04246 (National Science Centre, Poland) and statutory funds BS/PB-1-103-3010/11/P. PL-Grid infrastructure was used to carry out the computations.

References

1. F.L. HORN, M. STEINBERG, *Control of carbon dioxide emissions from a power plant (and use in enhanced oil recovery)*, Fuel, **61**, 415–422, 1982.
2. B.M. ABRAHAM, J.G. ASBURY, E.P. LYNCH AND A.P.S. TEOTIA, *Coal-oxygen process provides CO₂ for enhanced recovery*, Journal of Oil & Gas, **80**, 68–70, 1982.
3. G. SCHEFFKNECHT, L. AL-MAKHADMEH, U. SCHNELL, J. MAIER, *Oxy-fuel coal combustion — A review of the current state of the art*, International Journal of Greenhouse Gas Control, **5**, 16–35, 2011.
4. R. CABRA, T. MYRVOLD, J.Y. CHEN, R.W. DIBBLE, A.N. KARPETIS, R.S. BARLOW, *Simultaneous laser Raman-Rayleigh-Lif measurements and numerical modeling results of a lifted turbulent H₂/N₂ jet flame in a vitiated coflow*, Proceedings of the Combustion Institute, **29**, 1881–1888, 2002.
5. R. SEISER, K. SESHADRI, *The influence of water on extinction and ignition of hydrogen and methane flames*, Proceedings of the Combustion Institute, **30**, 407–414, 2005.
6. A. ROSIAK, A. TYLISZCZAK, *LES-CMC simulations of a turbulent hydrogen jet in oxy-combustion regimes*, International Journal of Hydrogen Energy, **41**, 9705–9717, 2016.
7. M.A. MUELLER, T.J. KIM, R.A. YETTER, F.L. DRYER, *Flow reactor studies and kinetic modeling of the H₂/O₂ reaction*, International Journal of Chemical Kinetics, **31**, 113–125, 1999.
8. J. LI, Z. ZHAO, A. KAZAKOV, F. L. DRYER, *An updated comprehensive kinetic model of hydrogen combustion*, International Journal of Chemical Kinetics, **36**, 566–575, 2004.
9. P. WARZECHA, A. BOGUSLAWSKI, *LES and RANS modeling of pulverized coal combustion in swirl burner for air and oxy-combustion technologies*, Energy, **66**, 732–743, 2014.

10. P. WARZECHA, A. BOGUSLAWSKI, *Simulations of pulverized coal oxy-combustion in swirl burner using RANS and LES methods*, Fuel Processing Technology, **119**, 130–135, 2014.
11. J. PEDEL, J.N. THORNOCK, P.J. SMITH, *Ignition of co-axial turbulent diffusion oxy-coal jet flames: Experiments and simulations collaboration*, Combustion and Flame, **160**, 1112–1128, 2013.
12. J. ZHANG, K. KELLY, E. EDDINGS, J. WENDT, *Ignition in 40 kW co-axial turbulent diffusion oxy-coal jet flames*, Proceedings of the Combustion Institute, **33**, 3375–3382, 2011.
13. A. GARMORY, E. MASTORAKOS, *Numerical simulation of oxy-fuel jet flames using unstructured LES-CMC*, Proceedings of the Combustion Institute, **35**, 1207–1214, 2015.
14. S. NAVARRO-MARTINEZ, A. KRONENBURG, *Conditional moment closure for large eddy simulations*, Flow, Turbulence and Combustion, **87**, 377–406, 2011.
15. A. GARMORY, E. MASTORAKOS, *Capturing localised extinction in Sandia Flame F with LES-CMC*, Proceedings of the Combustion Institute, **33**, 1673–1680, 2011.
16. I. STANKOVIĆ, E. MASTORAKOS, B. MERCI, *LES-CMC simulations of different auto-ignition regimes of hydrogen in a hot turbulent air co-flow*, Flow, Turbulence and Combustion, **90**, 583–604, 2013.
17. A. TYLISZCZAK, *Assessment of implementation variants of conditional scalar dissipation rate in LES-CMC simulation of auto-ignition of hydrogen jet*, Archives of Mechanics, **65**, 97–129, 2013.
18. A. TRIANTAFYLIDIS, E. MASTORAKOS, R.L.G.M. EGGELS, *Large eddy simulations of forced ignition of a non-premixed bluff-body methane flame with conditional moment closure*, Combustion and Flame, **156**, 2328–2345, 2009.
19. A. TYLISZCZAK, B.J. GEURTS, *Parametric analysis of excited round jets-numerical study*, Flow, Turbulence and Combustion, **93**, 221–247, 2014.
20. A. TYLISZCZAK, *Multi-armed jets: A subset of the blooming jets*, Physics of Fluids, **27**, 1–7, (041703), 2015.
21. A. TYLISZCZAK, *LES-CMC study of an excited hydrogen flame*, Combustion and Flame, **162**, 3864–3883, 2015.
22. B.J. GEURTS, *Elements of Direct and Large-Eddy Simulation*, Edwards Publishing, 2003.
23. P. SAGAUT, *Large Eddy Simulation for Incompressible Flows*, Springer, 2001.
24. A.W. VREMAN, *An eddy-viscosity subgrid-scale model for turbulent shear flow: Algebraic theory and applications*, Physics of Fluids, **16**, 3670–3681, 2004.
25. Y.A. KLIMENKO, R.W. BILGER, *Conditional moment closure for turbulent combustion*, Progress in Energy and Combustion Science, **25**, 595–687, 1999.
26. T. POINSOT, D. VEYNANTE, *Theoretical and Numerical Combustion*, Edwards, 2001.
27. A. TRIANTAFYLIDIS, E. MASTORAKOS, *Implementation issues of the conditional moment closure model in large eddy simulations*, Flow, Turbulence and Combustion, **84**, 481–512, 2010.
28. S. NAVARRO-MARTINEZ, A. KRONENBURG, F. DI MARE, *Conditional moment closure for large eddy simulations*, Flow, Turbulence and Combustion, **75**, 245–274, 2005.

-
29. A.W. COOK, J.J. RILEY, *A subgrid model for equilibrium chemistry in turbulent flows*, *Physics of Fluids*, **6**, 2868–2870, 1994.
 30. N. BRANLEY, W. JONES, *Large eddy simulation of a turbulent non-premixed flame*, *Combustion and Flame*, **127**, 1914–1934, 2001.
 31. I.S. KIM, E. MASTORAKOS, *Simulations of turbulent lifted jet flames with two-dimensional conditional moment closure*, *Proceedings of the Combustion Institute*, **30**, 911–918, 2005.
 32. I.S. KIM, E. MASTORAKOS, *Simulations of turbulent non-premixed counterflow flames with first-order conditional moment closure*, *Flow, Turbulence and Combustion*, **76**, 133–162, 2006.
 33. A. TYLISZCZAK, D.E. CAVALIERE, E. MASTORAKOS, *LES/CMC of blow-off in a liquid fueled swirl burner*, *Flow, Turbulence and Combustion*, **92**, 237–267, 2013.
 34. A. TYLISZCZAK, *A high-order compact difference algorithm for half-staggered grids for laminar and turbulent incompressible flows*, *Journal of Computational Physics*, **276**, 438–467, 2014.
 35. A. TYLISZCZAK, *High-order compact difference algorithm on half-staggered meshes for low Mach number flows*, *Computers & Fluids*, **127**, 131–145, 2016.
 36. P.N. BROWN, G.D. BYRNE, A.C. HINDMARSH, *VODPK: A Variable-Coefficient Ordinary Differential Equation Solver with the Preconditioned Krylov method GMRES for the Solution of Linear Systems*, available from Netlib, 1994.
 37. P.N. BROWN, G.D. BYRNE, A.C. HINDMARSH, *VODE: A variable-coefficient ODE solver*, *SIAM Journal on Scientific and Statistical Computing*, **10**, 1038–1051, 1989.
 38. P.N. BROWN, A.C. HINDMARSH, *Reduced storage matrix methods in stiff ODE systems*, *Applied Mathematics and Computation*, **31**, 40–91, 1989.
 39. S.F. AHMED, E. MASTORAKOS, *Spark ignition of lifted turbulent jet flames*, *Combustion and Flame*, **146**, 215–231, 2006.
 40. C.J. LAWN, *Lifted flames on fuel jets in co-flowing air*, *Progress in Energy and Combustion Science*, **35**, 1–30, 2009.

Received April 12, 2016; revised version November 15, 2016.
